ELSEVIER

Journal of Power Sources 70 (1998) 70–77

JOURNAL OF POWER SOURCES

Cathodic properties of a lithium-ion secondary battery using $LiCoO_2$ prepared by a complex formation reaction

Euh-Duck Jeong, Mi-Sook Won, Yoon-Bo Shim *

Department of Chemistry, Pusan National University, Pusan 609-735, South Korea

Received 27 March 1997; accepted 19 May 1997

Abstract

A $LiCoO_2$ precursor is prepared by a complex formation reaction in a solution that contains LiOH, $Co(NO_3)_2$, and humic acid it is used as a cathode for a lithium-ion rechargeable battery. Layered $LiCoO_2$ powders are prepared in air at 700 or 850°C after preheating the precursor at 350 and 450°C, respectively. X-ray diffraction spectra of the powders display a high intensity (003) peak and two low intensity (104) and (101) peaks. This indicates that the powders are well crystallized. Cyclic voltammetry, a galvanostatic charge/discharge experiment, and impedance spectroscopy are used to characterize the $LiCoO_2$ electrode in a 1 M $LiClO_4$/propylene carbonate electrolyte solution during the intercalation/de-intercalation of lithium ions through the electrode. The voltammogram recorded at a scan rate of 0.01 mV s^{-1} shows a set of redox waves that are caused by the de-intercalation/intercalation of lithium ions through the electrode. A cell, composed of a $LiCoO_2$ cathode and a Li anode, shows an initial discharge specific capacity of 112.5 mA h g^{-1} at a current density of 1 mA cm^{-2} (43.25 mA g^{-1}) between 3.6 and 4.2 V vs. Li/Li^+ electrode. 100 charge/discharge cycles were achieved for a cell composed of a $LiCoO_2$ cathode and graphite (MCMB 6-28) anode separated by Cellgard 2300. X-ray diffraction, charge/discharge, and cyclic voltammetric data shows that there is only a single phase reaction below 4.3 V during charge/discharge for a electrode prepared at 700°C. The diffusivity of lithium ions, D_{Li}^{+}, as determined by AC. impedance, is 5.2×10^{-12} m^2 s^{-1}.

Keywords: Cyclic voltammetry; $LiCoO_2$; Solution phase reaction; Lithium-ion battery; Humic acid; A.C. impedance

1. Introduction

$LiCoO_2$ [1–6] has received much attention as a suitable cathode material for lithium secondary batteries. It is one of the $LiMO_2$ (M = V, Cr, Co, Ni) series that has the layered rock salt structure with a basic structure composed of a closed-packed network of oxygen [3]. The range of the theoretical intercalation/de-intercalation of lithium ions through the $Li_{1-x}CoO_2$ structure is $0 < x < 1$ and the specific capacity is 274 mA h g^{-1}. The use of $LiCoO_2$ as a cathode material for lithium-ion batteries was first proposed by Mizushima et al. [1]. Later, Sony Energy Tech. in Japan commercialized the $LiCoO_2$/C system as a secondary battery [2]. Subsequently, many studies have been carried out [3–9] for the preparation of $LiCoO_2$, electrochemical properties, etc. to detain much better charge/discharge properties. Most have investigated $LiCoO_2$ with solid-phase reactions. The latter reactions have disadvantages such as non-homogeneity of particles, abnormal grain growth, and poor control of stoichiometry. In order to improve these and to lower the synthesis temperature of a precursor that has homogeneous and smaller grain size, solution-phase reactions have been used rather than solid-phase reactions. Yoshio et al. [10] prepared $LiCoO_2$ by heat treatment at 900°C with a solution-phase reaction. The first discharge capacity in the potential range of 3.7 to 4.3 V was larger than that obtained by the conventional solid-phase reaction. In addition, Ogihara et al. [11] made fine powders that employed an ultrasonic spray decomposition technique. They dissolved $LiNO_3$ and $Co(NO)_3 \cdot 6H_2O$ in an aqueous solution, then treated a mist of the solution that was generated by an ultrasonic vibrator at 900°C. In this method, a spherical $LiCoO_2$ powder was formed in a much shorter time than that experienced with solid-phase reactions. The resulting current capacity was 80 ~ 110 mA h g^{-1} which is comparable to that resulting from other solid-phase reactions with carbonate. By contrast, little attention has been paid to the solution phase-reaction for

* Corresponding author.

0378-7753/98/$19.00
PII S0378-7753(97)02667-0

$LiCoO_2$ [11–13], although several groups have reported the preparation of lithium manganese oxides via a solution-phase reaction [14–16].

Thus, we report here a low-temperature synthesis to obtain homogeneous $LiCoO_2$ by means of a solution-phase reaction through the complex formation reaction between humic acid and cobalt and/or lithium ions in an aqueous solution. Humic acid is well known as one of the important multidentate complexing agents for metal ions in natural waters and interstitial waters of soils and sediments. It has a molecular structure that easily complexes metal ions and is composed of aromatic rings substituted by carboxyl, phenolic hydroxyl, and alkyl groups and interconnected through aliphatic, alicyclic, and ether linkages [17,18].

To characterize the $LiCoO_2$ cathode prepared in the present study, electrochemical experiments were undertaken by using cyclic voltammetry and charge/discharge experiments under various experimental conditions. Changes in its structure with a variation in the charging capacity were determined using XRD, and A.C. impedance spectroscopy for charge/discharge experiments with constant potential and current.

2. Experimental

2.1. Preparation of $LiCoO_2$ precursor

A 25 g sodium salt of humic acid (Aldrich) was dissolved in 50 ml water purified by a Milli-Q system (18 MΩ). This solution was slowly mixed with a 150 ml 0.1 M HCl solution for 1 h at 50°C, then washed and dried. A 200 ml aqueous solution of 50.4 g $LiOH \cdot H_2O$ and humic acid solution was prepared with stirring until complete reaction occurred at room temperature. The metal complex precursor was prepared by adding 400 ml of aqueous solution containing 291.03 g $Co(No)_3 \cdot 6H_2O$ to the above solution. The precursor was obtained as a gel that was concentrated by evaporating the solution. The gel was ignited in a furnace for 6 h at 350°C and then 12 h at 450°C. The final $LiCoO_2$ powder was obtained by heat treatment of the precursor, twice, at 700 or 850°C, respectively, in a tube-type furnace under a stream of air. The synthesis of the $LiCoO_2$ powder is summarized in Fig. 1. To confirm the quality of the $LiCoO_2$ electrode prepared in the present experiment, the characteristics of the electrode were compared with those of standard $LiCoO_2$ powder purchased from Foot Mineral.

2.2. Preparation of electrode and cell

The cathode was prepared by coating the following mixtures on the current-collector: 85%(w/w) of $LiCoO_2$, 10%(w/w) of acetylene black, and 5%(w/w) polyvinylidene fluoride (PVDF) in *n*-Methyl pyrrolidone (NMP). After coating the mixture on a 1 cm^2 stainless-steel 316 ex-met by tape casting, the NMP was evaporated. The electrode was then dried under vacuum for 24 h at 120°C. The weight of each electrode was 20 ~ 25 mg. Lithium metal ribbon (Aldrich) pressed on a stainless-steel 316 ex-met was used both as the counter and the reference electrodes. The cell consisted of a $LiCoO_2$ working electrode, Li counter and reference electrodes, and a 1 M $LiClO_4$/propylene carbonate (PC) electrolyte solution (Battery grade by Mitsubishi Petrochemical) under Ar atmosphere at room temperature. The glass test cell was used to record cyclic voltammograms (CVs) and A.C. impedance spectra, and a two-electrode system was employed in galvanostatic charge/discharge experiments. Charge/discharge tests for a real lithium-ion battery were performed on a cylindrical type (electrode size: 50 × 500 mm^2) cell that comprised a LT-$LiCoO_2$ cathode and the graphite anode, which was made of MCMB6-28 (Osaka gas), in 1 M $LiClO_4$ EC/DMC (50% volume ratio) solution.

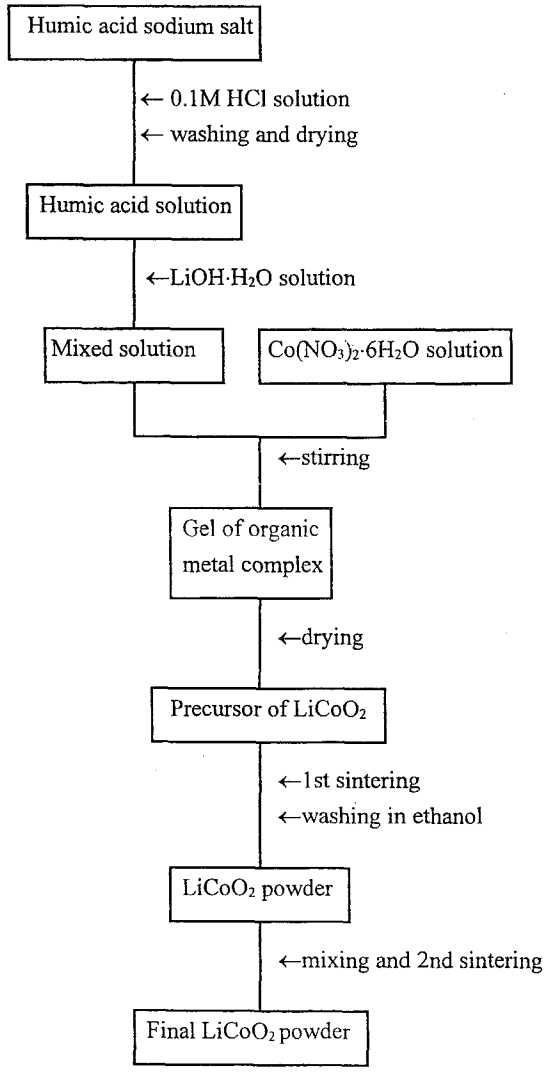

Fig. 1. Schematic diagram for synthesis of $LiCoO_2$.

2.3. Instruments

Thermogravimetry/differential thermal analysis (TG/DTA) were performed at a heating rate of 10°C min^{-1} up to 900°C in air using a Seiko Instrument (Model SSC/5200 SII) analyzer. X-ray diffraction (XRD) structure analyses of $LiCoO_2$ powders were carried out using a Rigaku X-ray diffractometer (D/Max) with CuK_α (1.5405 Å) radiation monochromated with a Ni-filter at a scanning range from 10 to 80° (+2 θ). Scanning electron micrographs for $LiCoO_2$ electrodes were obtained with a Hitachi Model S-2400 Scanning Electron Microscope (SEM). CVs were recorded employing a PAR Model 273 Potentiostat/Galvanostat (EG&G) with a Kipp and zonen X–Y recorder. Experiments for specific capacity vs. cycleability, properties of charge/discharge, and open-circuit voltage (OCV) were performed with a PAR 363 Potentiostat/Galvanostat interfaced with an IBM-compatible personal computer and an in-house software program. Impedance measurements were obtained with a PAR Model 273A Potentiostat/Galvanostat (EG&G) coupled to a EG &G 5201 Lock-in amplifier. Impedance spectra were recorded under potentiostatic control of the cell voltage as well as galvanostatic control by applying an A.C. voltage of 5 mV-rms amplitude over the frequency range 100 kHz to 20 MHz or 100 kHz to 10 MHz after the electrode attained an equilibrium potential. The impedance spectrometer was controlled by an IBM-compatible Pentium computer, and the data were analyzed in terms of an equivalent circuit by employing software supplied by EG&G PAR.

3. Results and discussion

3.1. TG/DTA and XRD patterns of the $LiCoO_2$ precursor

Optimum heat-treatment temperatures for preparing $LiCoO_2$ powders were determined with thermal analysis techniques. Fig. 2a and b shows TG and DTA curves for the precursor (a mixture of $Co(NO)_3 \cdot 6H_2O$, LiOH, and humic acid), while Fig. 2c and d curves for $Co(NO)_3 \cdot 6H_2O$ and humic acid, respectively. The total weight loss (as shown in Fig. 2b was observed to be about 57.3% between 200 and 900°C. The first exothermic peak at 306°C (see Fig. 2a) is due to the decomposition of mainly cobalt nitrate and part of the functional groups of humic acid. This was confirmed by TG curves that were separately recorded for $Co(NO)_3 \cdot 6H_2O$ and humic acid (see Fig. 2c and d). The weight loss starts at 60°C and is completed at around 250°C for $Co(NO)_3 \cdot 6H_2O$. By contrast, the weight loss in humic acid begins at around 60°C and almost finishes at 500°C, there is a small loss at around 600°C. The DTA curve for the $LiCoO_2$ precursor shows a second exothermic peak at 433°C this was small side peaks due to the thermal decomposition of humic acid between 450 and 630°C. The crystallization of the hexagonal phase $LiCoO_2$ takes place from about 650°C; this was confirmed by XRD phase analysis.

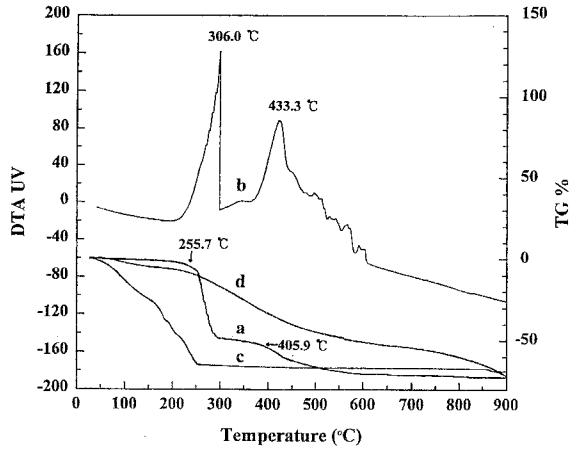

Fig. 2. TG/DTA curves for decomposition of (a,b) HA complex, (c), TG of $Co(NO_3)_2 \cdot 6H_2O$, (d) humic acid.

The solution-phase reaction required a lower heat-treatment temperature to prepare $LiCoO_2$, which was determined with TG/DTA. The XRD pattern of the $LiCoO_2$ precursor prepared at 700°C was the same as that given by the JCPDS (joint committee on powder diffraction standards) card. This indicates that the crystallization is completed at about 700°C. Table 1 shows the observed lattice parameters of $LiCoO_2$ powders together with those cited in the literature [4], such as the a and c values, line intensities of $I(003)$, $I(104)$), and a/c ratios. The XRD patterns of the $LiCoO_2$ powders heat-treated separately, at 700°C (LT-$LiCoO_2$) and 850°C (HT-$LiCoO_2$) in an air stream, are the same and equivalent to those reported previously [4]. The Miller indexes indicates that the powder has a pure hexagonal structure with an $R3m$ space group. Using the solution-phase reaction method, Yoshio et al. [10] obtained $LiCoO_2$ powders that had a strong intensity of the (003) line. Generally, the (003) line intensity decreases when an M atom partially occupies part of the octahedral sites of the lithium layer in $LiMO_2$ (M = Co,

Table 1
Structural analysis of $LiCoO_2$ powders

Samples	Lattice parameters (hexagonal)		c/a	Intensity ratio of $I(003)/I(104)$
	a (Å)	c (Å)		
LT-$LiCoO_2$	2.809	13.972	4.98	6.70
HT-$LiCoO_2$	2.818	14.075	4.99	8.09
CFM-$LiCoO_2^a$ powder	2.819	14.052	4.99	1.94
FMC-$LiCoO_2^b$ powder	2.815	14.009	4.98	3.641
HT-LiCoO2[4] powder	2.818	14.060	4.99	2.83

[a]$LiCoO_2$ of Cyprus Foot Mineral. [b]$LiCoO_2$ of Foot Mineral.

Ni, V and Cr). In the results presented here, the strongest peak at the Miller index (003) is observed in the samples obtained at 700 and 850°C. This result implies that the lithium and cobalt layers are well spaced in the rock salt structure, and suggests that the well-crystallized $LiCoO_2$ can be obtained even at a lower heat-treatment temperature than that used in other studies [3,5,7,8]. The scanning electron microscopic (SEM) studies showed that the particles were smooth. The particle size of sample powders prepared at 700°C was less than 3 μm. The crystal surface of HT-$LiCoO_2$ powder was slightly rougher and more irregular than that of LT-$LiCoO_2$.

3.2. Cyclic voltammetric behavior of $LiCoO_2$ electrode

Cyclic voltammograms between 3.78 and 4.0 V vs. Li/Li^+ electrode for LT–$LiCoO_2$ at a scan rate of 0.01 mV s^{-1} are presented in Fig. 3a. The cathodic peak current is larger than that for the corresponding anodic and this indicates that the redox process is irreversible and that Li ions de-intercalated at a potential higher than 4.2 V are irreversibly re-intercalated during the cathodic reaction. This lowers the initial charge/discharge efficiency. This behavior may be due to the fact that as the Li ions are de-intercalated from the $LiCoO_2$ crystal, Co^{3+} is oxidized to Co^{4+} which increases the concentration of Co^{4+} in the $LiCoO_2$ at high potentials. This is likely to destroy the crystal structure of the electrode and, hence, the reversibility of the cell. This has been proposed by Reimer and Dahn [3], as well as by Mizushima et al. [1] who observed a broadening of the XRD peak of $Li_{0.33}CoO_2$. Nevertheless, such behavior has little effect on the operation of a lithium-ion battery employing the $LiCoO_2$ electrode because the irreversible capacity loss can be ignored at a potential of about 4.2 V.

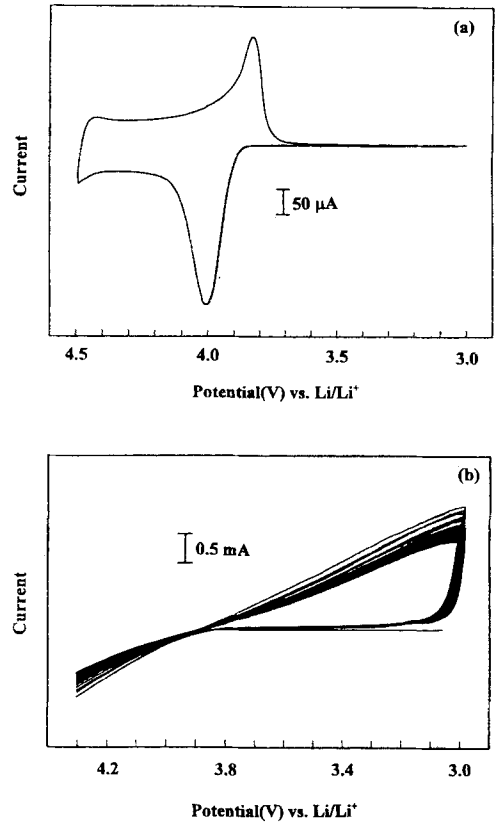

Fig. 3. Cyclic voltammograms of LT–$LiCoO_2$ electrodes: (a) scan rate 0.01 mV s^{-1}, potential range 3.0 to ~4.5 V; (b) 2 mV s^{-1}, potential range 3.0 to ~4.3 V.

The CV data are comparable with the results of the following research groups. Dreher et al. [19] obtained CVs recorded for a disc-type $LiCoO_2$ electrode at a scan rate of 0.05 mV s^{-1} and observed three peaks at about 3.97, 4.08 and 4.18 V during the oxidation reaction, and 4.15, 4.05 and 3.86 V during the reduction reaction. Uchida and Sato [9] also obtained CVs with three well-defined anodic peaks at about 3.95, 4.1 and 4.2 V, and cathodic peaks at 4.18, 4.07 and 3.9 V at the scan rate of 0.1 mV s^{-1} for a flag-type $LiCoO_2$/Au electrode in 1 M $LiClO_4$/PC. In addition, CVs recorded for commercialized $LiCoO_2$ powders obtained from Cyprus Foot Mineral as the reference material in this study displayed three redox peaks as other $LiCoO_2$ electrodes, all of which were synthesized by solid-phase reactions. The three redox peaks in the CVs must be the result of phase transition and/or cation disorder in the structure. Reimer and Dahn [3] have suggested that the subtle features in the $-dx/dV$ curve, corresponding to minor peaks in the CV, are due to phase transitions between ordered and disordered lithium-ion arrangements in the CoO_2 framework. By contrast, Yazami et al. [12] have suggested that other minor peaks observed in the CV for the $LiCoO_2$ electrode are due to cation disorder in the structure and anion adsorption on surface impurities, which was prepared by a solution-phase reaction at low temperature using cobalt acetate and lithium acetate.

The CV patterns of a $LiCoO_2$ electrode synthesized by a solution-phase reaction using humic acid and heat-treated at low temperature (LT-$LiCoO_2$) are quite different from those in which the CV shows only one redox peak. This indicates that the LT-$LiCoO_2$ electrode experiences a single phase transition process during charge/discharge between 3.0 and 4.3 V, behavior that is similar to the result for LT-$LiCoO_2$ electrode reported by Gummow et al. [4] where the lithium insertion and extraction reactions are also one-step processes. To examine the cycleability and redox properties at a faster scan rate, CVs were recorded continuously at a scan rate of 2 mV s^{-1}. The resulting CVs between 3.0 and 3.4 V for an LT-$LiCoO_2$ electrode are shown in Fig. 3b. The peak potentials are shifted more irreversibly at this scan rate. The CVs indicates that the $LiCoO_2$ electrode prepared in the present work has a good cycleability and excellent properties as cathode material for lithium-ion secondary batteries. For 100 cycles of the oxidation/reduction test, the height of the redox peaks

reduced gradually during the first 15 cycles, but then remained constant.

3.3. XRD patterns for a $LiCoO_2$ electrode during potential cycling

To describe the structural change of $LiCoO_2$ during lithium de-intercalation, an XRD experiment was performed ex situ, in which XRD patterns were recorded during oxidizing the electrode at a current density of 0.2 mA cm^{-2}. The hexagonal lattice parameters are given in Fig. 4 as a function of x in $Li_{1-x}CoO_2$. The (003) peak shifted to a lower Bragg angle at $x < 0.4$, which means that the c-axis was elongated as the de-intercalation proceeded to the $x = 0.4$ state and then became constant over this state. This is due to the fact that the spaces of the layer increase as the lithium de-intercalation proceeds because the layer-structured, $LiCoO_2$ causes the coulombic repulsion of adjacent oxygen atom layers. Reduction of the c-axis values in the region where $x > 0.6$ is the result of greatly disordered layers as a considerable amount of lithium ions were de-intercalated. It can be assumed that the phase transitions between ordered and disordered lithium ions that occur in the CoO_2 framework are due to an unstable layered structure caused by the formation of an excess of Co(IV) ions. On the other hand, there is no change in the a-axis values during lithium intercalation. This is consistent with the results of Ozuku and Ueda [5].

3.4. Charge / discharge properties of $LiCoO_2$ electrode

The initial charge/discharge curve, in terms of the cell voltage as a function of lithium concentration, x, for a $Li_{1-x}CoO_2$ electrode between 4.3 and 3.0 V at 0.2 mA

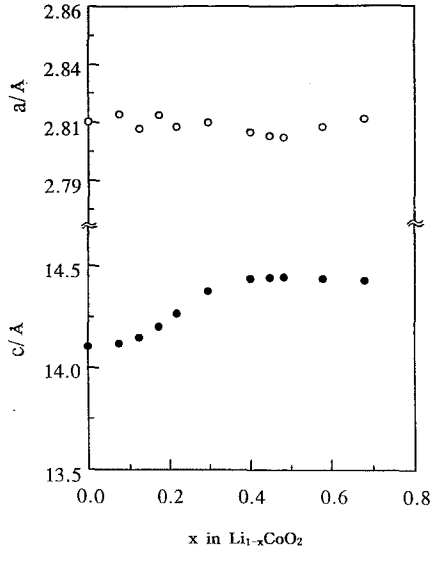

Fig. 4. Lattice parameters of a hexagonal unit cell at various charge densities as a function of x in $Li_{1-x}CoO_2$ obtained 700°C; (○) a-axis and (●) c-axis.

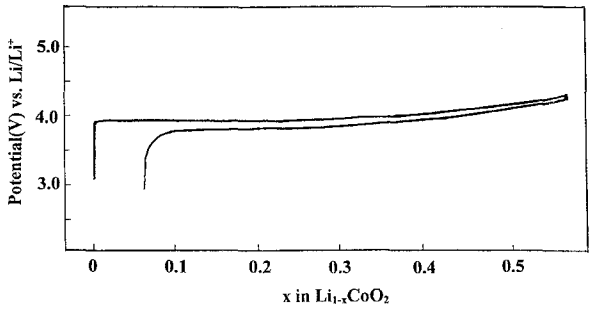

Fig. 5. Cell voltage as a function of x in $Li_{1-x}CoO_2$ for the initial charge/discharge of LT-$LiCoO_2$. Charge/discharge potentials applied between 4.30 and 3.0 V at 0.2 mA cm^{-2} (10.46 mA g^{-1}).

cm^{-2} (10.46 mA g^{-1}) are presented in Fig. 5. The lithium concentration has been calculated from the theoretical capacity and the total charge transferred LT-$LiCoO_2$ has a potential plateau at 3.97 3.9 V during intercalation and de-intercalation, respectively. This result is different from those indicates three plateaus [3,7]. As expected, the CV has a redox wave of the type shown in Fig. 3. A $LiCoO_2$/Li cell employing LT-$LiCoO_2$ has a high discharge capacity of 142.6 mA h g^{-1} and a charge capacity of 152.7 mA h g^{-1}. Only a single phase reaction occurs during the charge/discharge process, and the first charge/discharge coulombic efficiency is excellent (93.4%). The good properties should result from using a highly homogeneous and electrochemically active precursor synthesized in a solution phase and heated at low temperature. On the other hand, a HT-$LiCoO_2$/Li cell displays an initial charge/discharge capacity of 145.5/131.1 mA h g^{-1} with a 90.1% charge/discharge efficiency. These values are lower than those of the LT-$LiCoO_2$/Li. cell.

To confirm the above results, the variation in the open-circuit voltage as a function of x in $Li_{1-x}CoO_2$ were obtained with the cell off for 5 min and then on for 30 min in $LiCoO_4$/PC at a 0.2 mA cm^{-2}. The open-circuit voltage was constant to 3.9 V between $x = 0$ and $x = 0.4$ in $Li_{1-x}CoO_2$, but increased continuously with lithium composition, x, between $0.4 < x < 0.8$ in $Li_{1-x}CoO_2$ and the electrode reaction occurred as a single-phase reaction. The results are the same as the CV data discussed previously.

Fig. 6 is a plot of the capacity as a function of the number of charge/discharge cycles for LT-(a and b), CFM (c and d) and HT-$LiCoO_2$ (e and f) electrodes at 1 mA cm^{-2} over the potential range 4.2 to 3.6 V. The initial charge/discharge capacities are 112.5 and 99.5 mA h g^{-1}, respectively, and the coulombic efficiency is 88.5%. The capacity for the second cycle is 92.5 mA h g^{-1}, and there is 100% efficiency. For HT-$LiCoO_2$, the initial charge/discharge capacities are 100.7/72.9 mA h g^{-1} with an efficiency of 72.4% and 102/90 mA h g^{-1} with an efficiency of 88.2% for CFM-$LiCoO_2$. As expected, LT-$LiCoO_2$ gave the best capacity and efficiency.

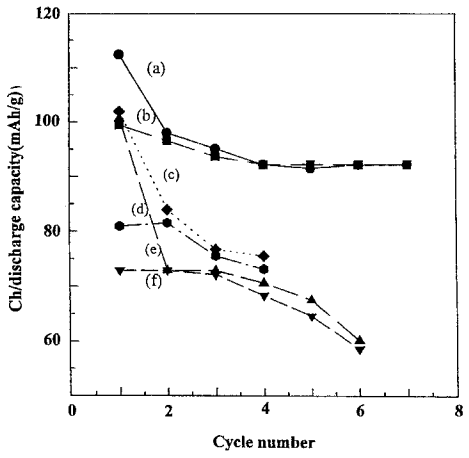

Fig. 6. Plot of variation of charge/discharge capacities of $LiCoO_2$ according to cycle number over potential range 4.2 to 3.6 V and at 1 mA cm^{-2}. Charge/discharge capacity values are, respectively, for (a,b) LT-$LiCoO_2$, (c,d) CFM-$LiCoO_2$, (e,f) HT-$LiCoO_2$.

To represent an actual battery system, the cycleability was examined for a cell composed of a $LiCoO_2$ cathode and a graphite (MCMB 6-28) anode separated by Cellgard 2300 with an electrolyte of 1 M $LiClO_4$ in EC/DMC solution. The charge/discharge experiments were performed over a potential range of 4.2 and 2.75 V at a current of 0.27 A. The capacity as a function of the number of cycles is given in Fig. 7. The discharge and charge capacity of the battery was 688 and 778 mA h, respectively, on the first cycle and the utility of the system was 110 mA h g^{-1} for the cathode and 274 mA h g^{-1} for the anode. With further cycling (100 cycles), the capacity dropped to 77% of the initial value with a charge/discharge efficiency of 98–99%. The reduction in capacity is probably caused by a physical defect in the electrode surface and inequivalence of the electrode materials with an increasing number of cycles.

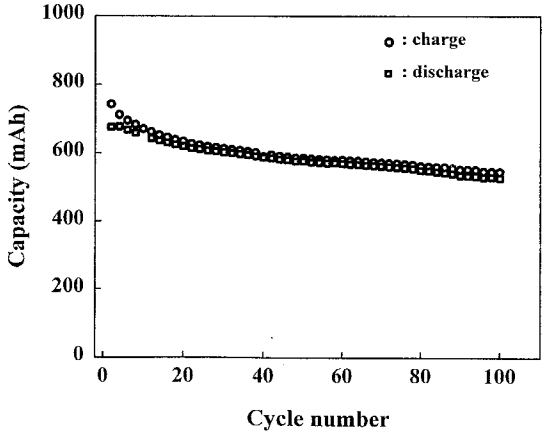

Fig. 7. Charge/discharge capacities of lithium-ion battery over potential range: 4.2 to 2.75 V.

3.5. A.C. impedance characterization of $LiCoO_2$ electrode

To understand the interface phenomena of the $LiCoO_2$ electrode, impedance spectra were obtained. The impedance spectrum recorded at an open-circuit voltage below 3.8 V displays an arc and a normal line to the x-axis in the regions of high and low frequencies, respectively, as shown in Fig. 8a. The arc and line corresponds to the charge-transfer resistance (R_{ct}) and the charge saturation process, respectively. Fig. 8b shows a typical Nyquist plot recorded for a $LiCoO_2$ electrode at various cathodic potentials (intercalation processes of Li ions) with variation from 4.3 to 3.0 V vs. Li/Li^+ electrode. As the applied potential goes from 4.3 to 3.8 V, which is around the peak potential in the CV, the second arc in the higher frequency range begins to appear from the set-up potential of the CV, which corresponds to the resistance caused by another charge-transfer process (R_{ad}) due to insertion/extraction of Li ions through the interface of the electrolyte/oxide electrode. While the inclined line in the lower frequency range below 50 MHz is attributable to a Warburg impedance that is associated with the diffusion of Li ions through the $LiCoO_2$ electrode. The R_{ad} of the second arc increases gradually with increasing resistance of the adsorption layer formed on the electrode surface by the formation of lithium layers due to the reduction of lithium ions [20,21]. Impedance spectra for a $LiCoO_2$ electrode at various oxidation potentials (de-intercalation process of lithium ions) with variation from 3.8 to 4.4 V vs. Li/Li^+ electrode are similar to the spectra recorded at the reduction potential, except for small differences in the values.

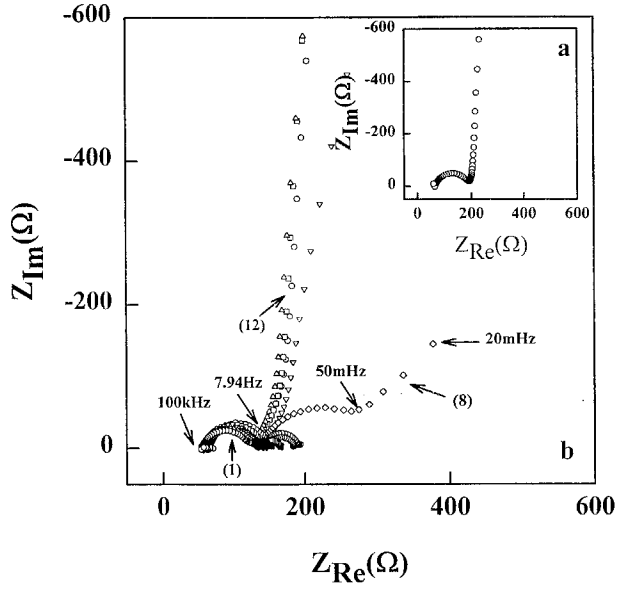

Fig. 8. Nyquist plots obtained for LT–$LiCoO_2$ electrode: (a) at open-circuit voltage; (b) at various reduction potentials at 4.3 (1), 4.2 (2), 4.1 (3), 4.0 (4), 3.95 (5), 3.9 (6), 3.85 (7), 3.8 (8), 3.7 (9), 3.6 (10), 3.3 (11), and 3.0 V (12). Measuring frequency range = 100 kHz to ~ 20 MHz.

Table 2
Values of the parameters of the equivalent circuit simulated for the impedance spectrum of a LT–$LiCoO_2$ electrode recorded in the positive voltage direction

$R_s(Q_1[R_1(Q_2[R_2Q_3])])$									
Oxidation potential, V	R_s, Ω	R_{ct}, Ω	Q_1		R_{ad}, Ω	Q_2		Q_3	
			Y_0, mho × 10^{-6}	n_1		Y_0, mho	n_2	Y_0, mho	n_3
3.80	61.23	60.35	18.43	0.8904	–	22	0.3604	–	–
3.90	61.93	65.83	23.34	0.8528	–	8.273	0.7302	–	–
3.95	62.27	64.27	23.66	0.8513	106.5	7.047	0.8497	–	–
4.00	62.74	60.55	22.76	0.8625	58.37	6.088	0.8620	–	–
4.05	63.61	60.07	22.49	0.8634	38.09	5.686	0.8461	–	–
4.10	63.92	59.00	21.07	0.8684	28.19	5.828	0.7609	–	–
4.15	63.96	59.52	21.15	0.8679	20.60	5.561	0.7480	–	–
4.20	60.36	57.34	22.29	0.8682	12.74	4.323	0.8403	–	–
4.30	55.97	56.96	29.75	0.8392	13.40	4.952	0.7580	482.9	0.2765
4.40	57.65	60.08	37.84	0.8198	13.98	6.375	0.7549	56.52	0.2786

Table 2 shows the parameter values of the equivalent circuit for the impedance spectrum of a $LiCoO_2$ electrode. In this case, R_{ad} gradually decreases as the applied oxidation potential goes from 3.95 V to 4.2 V. This indicates that lithium ions easily move out from the inside of the electrode during the de-intercalation process compared with their insertion into the electrode during the intercalation process. As previously mentioned, this result is consistent with the CV result that shows a decrease in the internal resistance of the electrode at potentials beyond the oxidation peak. While a higher internal resistance in the lower oxidation potential region is attributable to increasing internal resistance with large degrees of lithium-ions de-intercalation.

We suggest an equivalent circuit for the spectra by using a CNLS (complex non-linear square) fitting analysis with commercialized software. This circuit is similar to that reported by Choi et al. [22] that was obtained with a galvanostatic intermittent titration technique (TITT). The behavior is also similar to that for an $LiMn_2O_4$ electrode [23], but is different to that for an $LiCoO_2$ thin layer electrode [24]. A Nyquist plot at a constant charge/discharge current was similar to the result obtained at various potentials (not shown) An impedance experiment was conducted in order to determine the chemical diffusivity, D_{Li+}, for the LT-$LiCoO_2$. The value of the chemical diffusivity, D_{Li+}, in $LiCoO_2$ was calculated by using the following relationship [21]:

$$Z_w = A_w \omega^{-1/2}(1-j),$$
$$A_w = \left(V_M/FA(2D)^{1/2}\right)(dV_{OCV}/dx). \quad (1)$$

where: V_M is the molar volume; (dV_{OCV}/dx) is the gradient of the open-circuit voltage against composition x at the bulk composition; F is the Faraday constant; A is the active surface area. In this case, the chemical diffusivity of $Li_{0.58}CoO_2$ (4.2 V) was calculated to be 5.2×10^{-12} m^2 s^{-1}, which is close to that given in previous reports [22,21].

4. Conclusions

The well-developed layered structure of $LiCoO_2$ obtained with humic acid in a solution-phase reaction displays a higher capacity than that prepared by a solid-phase reaction. $LiCoO_2$ gives excellent CV cycling behavior over the potential range between 3.0 and 4.3 V vs. a Li/Li^+ electrode. The $LiCoO_2$/Li cell provides a charge/discharge capacity of 173.1/151.4 mA h g^{-1} on the initial cycle at 0.4 mA cm^{-2} (12.75 mA g^{-1}) and the voltage range was between 4.55 and ~3.0 V. The $LiCoO_2$/Li cell displays an available discharge specific capacity of 112.5 to ~96.6 mA h g^{-1} at a current density of 1 mA cm^{-2} (43.25 mA g^{-1}) and a voltage range between 3.6 and ~4.2 V. The coulombic efficiency is 88.5% on the first cycle and 98.5 to ~100% at the 2nd to 7th cycles, respectively. The discharge and charge capacity of the lithium ion battery, composed of a LT-$LiCoO_2$ cathode and a graphite (MCMB 6-28) anode, is 688 and 778 mA h, respectively on the initial cycle. After 100 cycles, the capacity dropped to 77% of the initial value and showed a charge/discharge efficiency of 98–99%. The LT-$LiCoO_2$ electrode gives the best performance, as expected from CV studies. The resistance due to the adsorption of lithium ions into the oxide electrode decreases with increasing lithium content. The chemical diffusivity of Li^+ ions in $Li_{0.58}CoO_2$ is calculated to be 5.2×10^{-12} m^2 s^{-1}.

Acknowledgements

This work was supported by the Korean Science and Engineering Foundation, Grant No. 961-0304-030-2.

References

[1] K. Mizushima, P.C. Jones, P.J. Wiseman, J.B. Goodenough, Mater. Res. Bull. 15 (1980) 783.
[2] T. Nagaura, JEC Battery Newslett. 2 (1991) 17.
[3] J.N. Reimer, J.R. Dahn, J. Electrochem. Soc. 139 (1992) 2091.
[4] R.J. Gummow, M.M. Thackeray, W.I.F. David, S. Hull, Mater. Res. Bull. 27 (1992) 327.
[5] T. Ozuku, A. Ueda, J. Electrochem. Soc. 141 (1994) 2972.
[6] T. Ohzuku, A. Ueda, M. Nagayama, Y. Yasunou, H. Komori, Electrochim. Acta 38 (1993) 1159.
[7] E. Plichta, S. Slane, M. Uchiyama, M. Solomon, D. Chua, W.B. Ebner, H.W. Lin, J. Electrochem. Soc. 136 (1989) 1865.
[8] M. Antaya, J.R. Dahn, J.S. Preston, E. Rossen, J.N. Reimers, J. Electrochem. Soc. 140 (1993) 575.
[9] I. Uchida, H. Sato, J. Electrochem. Soc. 142 (1995) L139.
[10] M. Yoshio, H. Tanaka, K. Tominaga, H. Naguchi, J. Power Sources 40 (1992) 347.
[11] T. Ogihara, T. Yanagawa, N. Ogata, K. Yoshida, Y. Mizuno, S. Yonezawa, M. Takashima, N. Nagata, K. Ogawa, Denki Kagaku 61 (1993) 1339.
[12] R. Yazami, N. Lebrun, M. Bonneau, M. Molteni, J. Power Sources 54 (1995) 389.
[13] S.W. Chang, T.J. Lee, S.C. Lin, J.H. Jeng, J. Power Sources 54 (1995) 403.
[14] P. Barboux, J.M. Tarascon, F.K. Shokoohi, J. Solid State Chem. 94 (1991) 185.
[15] H. Hwang, P.G. Bruce, J. Electrochem. Soc. 141 (1994) L106.
[16] S. Bach, M. Henry, N. Barrier, J. Civage, J. Solid State Chem. 88 (1990) 325.
[17] C. Steelink, J. Chem. Education 40 (1963) 397.
[18] J. Buffle, F.L. Greter, W. Haerdi, Anal. Chem. 49 (1977) 216.
[19] J. Dreher, B. Haas, G. Hambitzer, J. Power Sources 43–44 (1993) 583.
[20] M.G.S.R. Thomas, P.G. Bruce, J.B. Goodennough, J. Electrochem. Soc. 132 (1985) 1521.
[21] M.G.S.R. Thomas, P.G. Bruce, J.B. Goodennough, Solid State Ionics 17 (1985) 13.
[22] Y.M. Choi, S.I. Pyun, J.S. Bae, S.I. Moon, J. Power Sources 56 (1995) 25.
[23] G. Pistoia, D. Zane, Y. Zhang, J. Electrochem. Soc. 142 (1995) 2551.
[24] T. Nishima, H. Sato, I. Uchida, The 36th Battery Symposium in Japan, 1995, pp. 7–8.